

Locally intense rain in Cuba under the influence of
Upper Cold Lows. Study of cases.

Author:

Osmany Lorenzo Amaro

osmanyloa@gmail.com

Upper Cold Lows (UCLs)



Figure 1.1: Average position of the TUTT in the months of July and August (Source: González, 2016).

- **(Alfonso *et al.*, 1990)** - Analysis of the relationship between UCLs and Severe Local Storms (TLS).
 - **(Laguardia, 2011)** - Realization of a climatology of the UCLs that influence the Cuban territory. Analysis of its characteristics and temporal and seasonal behavior.
- According to *Benhamrouche and Martín - Vide (2012)*, the UCLs are systems that encourage the occurrence of locally intense rain, which in turn can take place in a season due to local factors, not occurring in the surrounding territories (*Planos et al. ., 2004*).

Study area

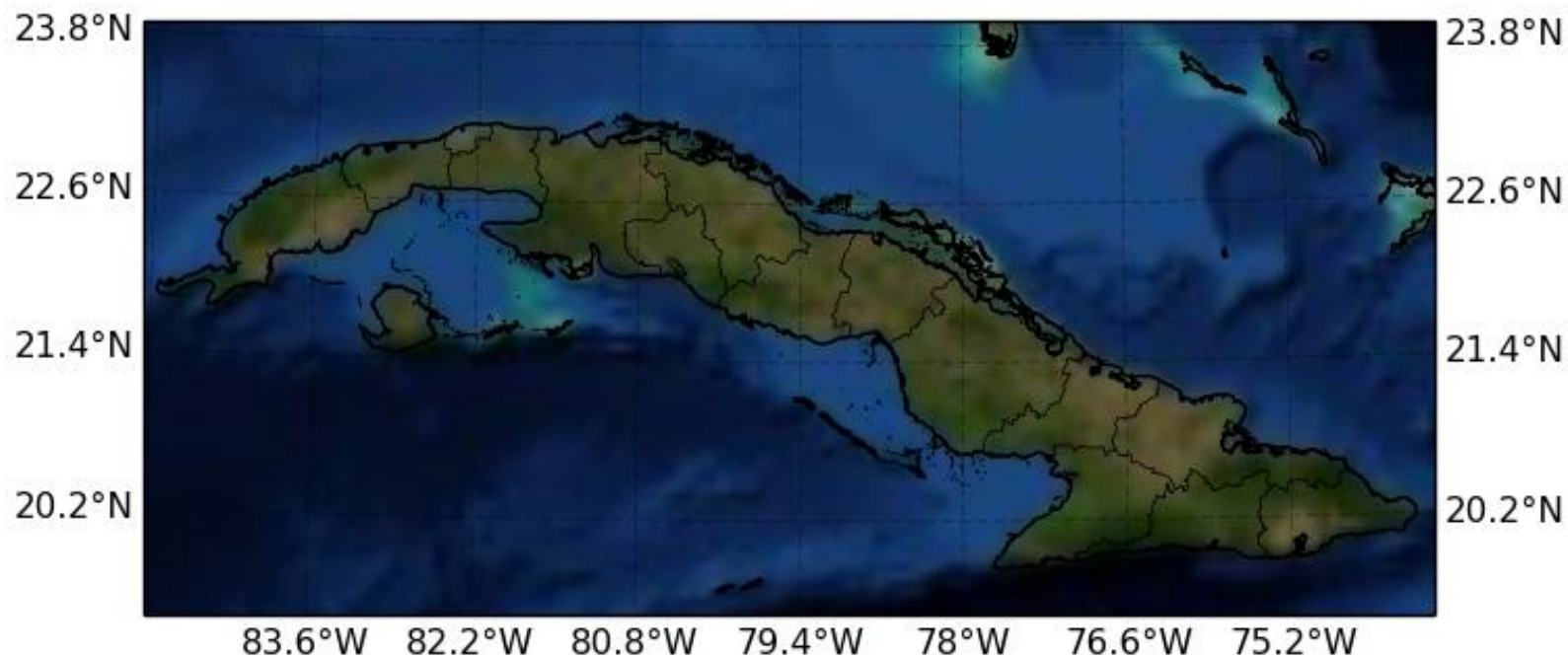


Figure 2.1: Study area used in the research.

Table 2.1: Spatial and temporal location of the cases of locally intense rain with their respective accumulations.

Días	Mes	Año	Localidad	Provincia	Latitud	Longitud	Valor de precipitación(mm)	Tiempo(horas)
2	7	2016	La Sierpe	Santi Spíritus	21.81°	-79.23°	101	24
3	7	2016	Colón	Matanzas	22.76°	-80.97°	176.5	24
16	8	2016	El Salvador	Guantánamo	20.33°	-75.36°	106	24
17	8	2016	Batabanó	Mayabeque	22.73°	-82.28°	61	12

Materials

- Three-hour data from the National Network of INSMET stations.
- Precipitation data from the INRH Rainfall Stations Network.
- Synoptic maps.
- Radar observations.
- Satellite images.

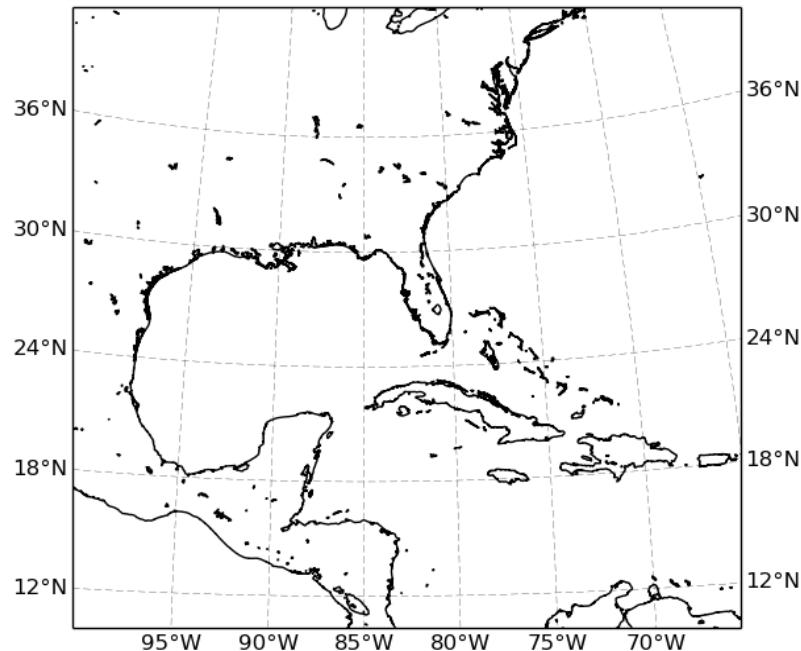


Figure 2.2: Synoptic space used.

Computing tools

- Grid Analysis and Display System (GrADS)
- Rapid Refresh (RAP)
- Weather Research and Forecast System (WRF) (SisPI)
- Python programming language (versions 2.7 and 3.6)
- SAGA and QGIS softwares

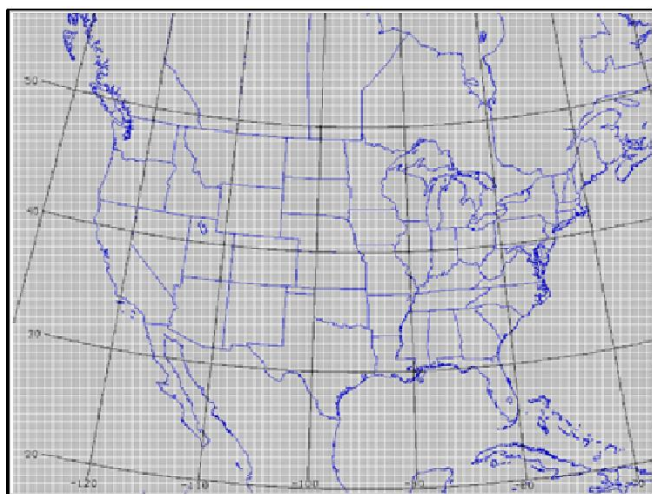


Figure 2.3: Domain of the RAP model used (Source: Gutierrez (2019)).

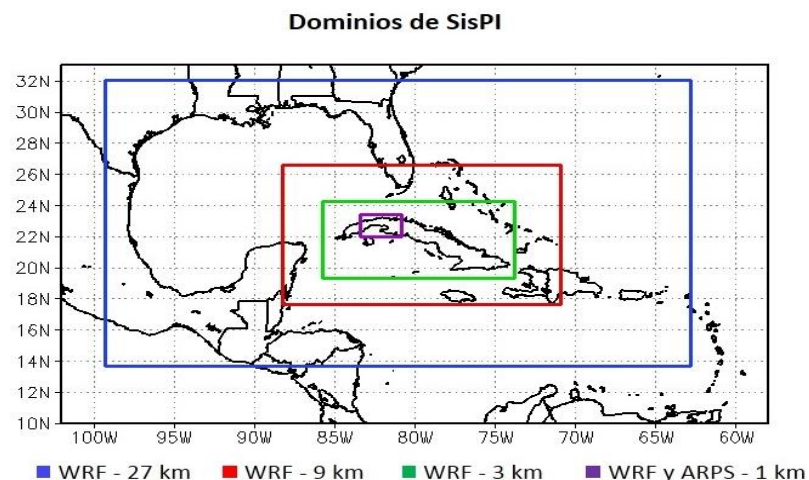


Figure 2.4: Simulation domains of the WRF model (Source: Sierra et al. (2017)).

Methods

- Analysis with the RAP model of the variables temperature, geopotential, wind force and vertical wind speed, from the surface to the level of 100 mb.
- Carrying out numerical surveys.
- Use of radical variables.
- Calculation of dynamic variables.

Component shear horizontal wind

$$|\vec{V}_c| = \sqrt{(u_2 - u_1)^2 + (v_2 - v_1)^2}$$

Divergence

$$\delta = \nabla_h \cdot \vec{V} = \left(\frac{\partial u}{\partial x} + \frac{\partial v}{\partial y} \right)$$

Vorticity

$$\zeta = \hat{k} \cdot (\nabla \times \vec{V}) = \left(\frac{\partial v}{\partial x} - \frac{\partial u}{\partial y} \right)$$

Synoptic description

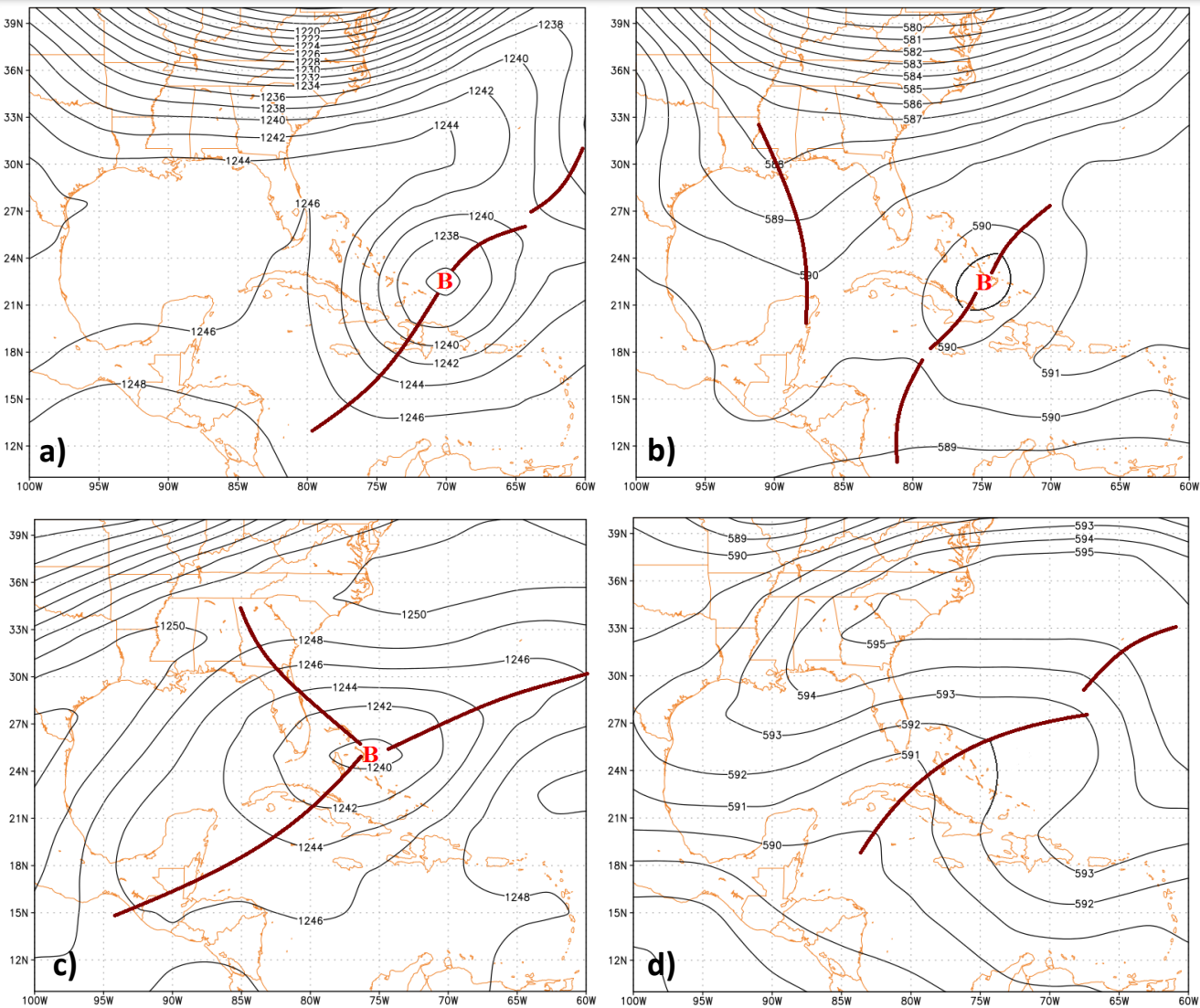


Figure 3.1: Geopotential height at levels 200 and 500 mb corresponding to June 30, 2016 at 0600 UTC (a) and (b) and August 17, 2016 at 1200 UTC (c) and (d).

Synoptic description

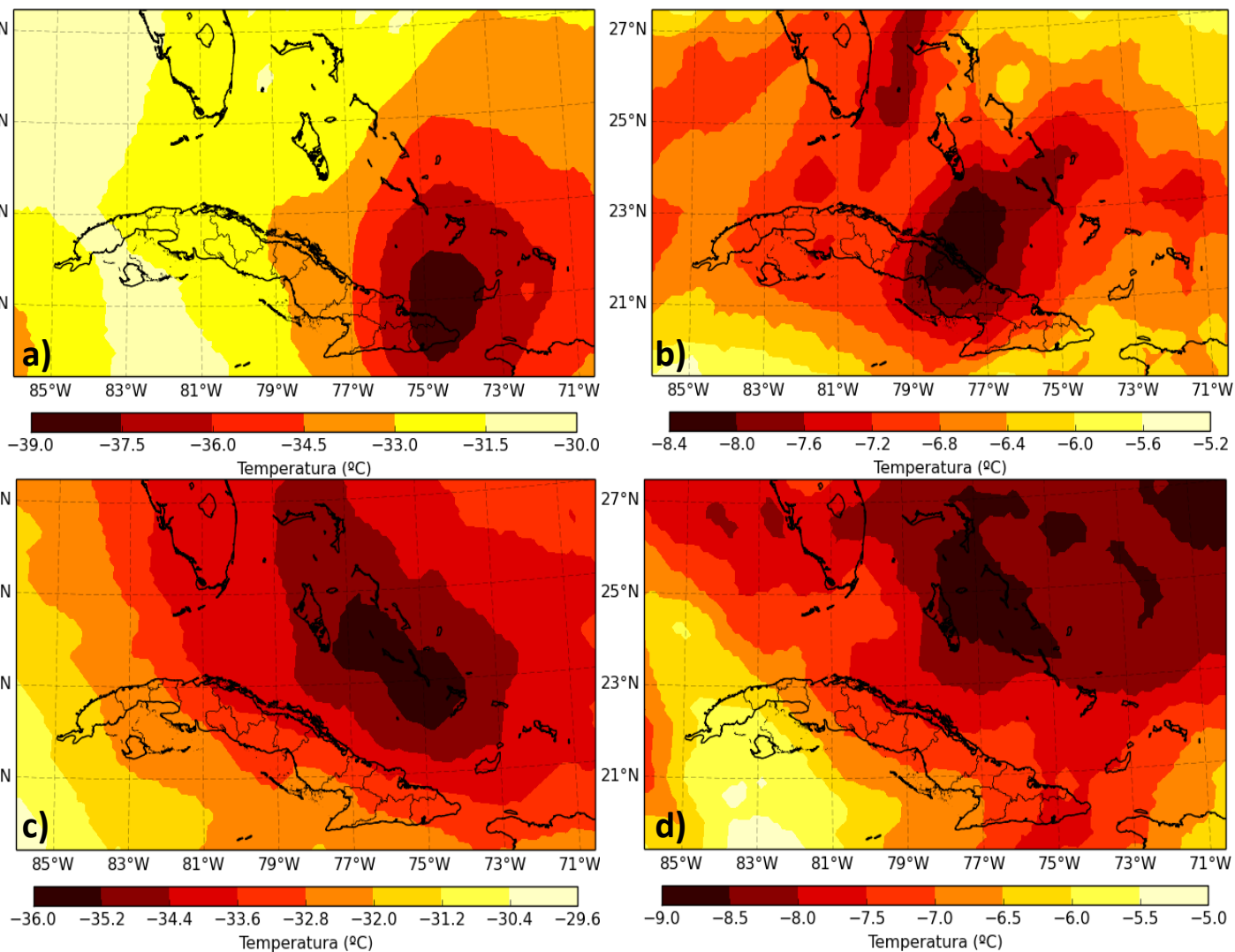


Figure 3.2: Temperature at the level of 300 and 500 mb corresponding to July 2, 2016 at 1400 UTC ((a) and (c)) and August 16, 2016 at 1300 UTC ((b) and (d)).

Synoptic description

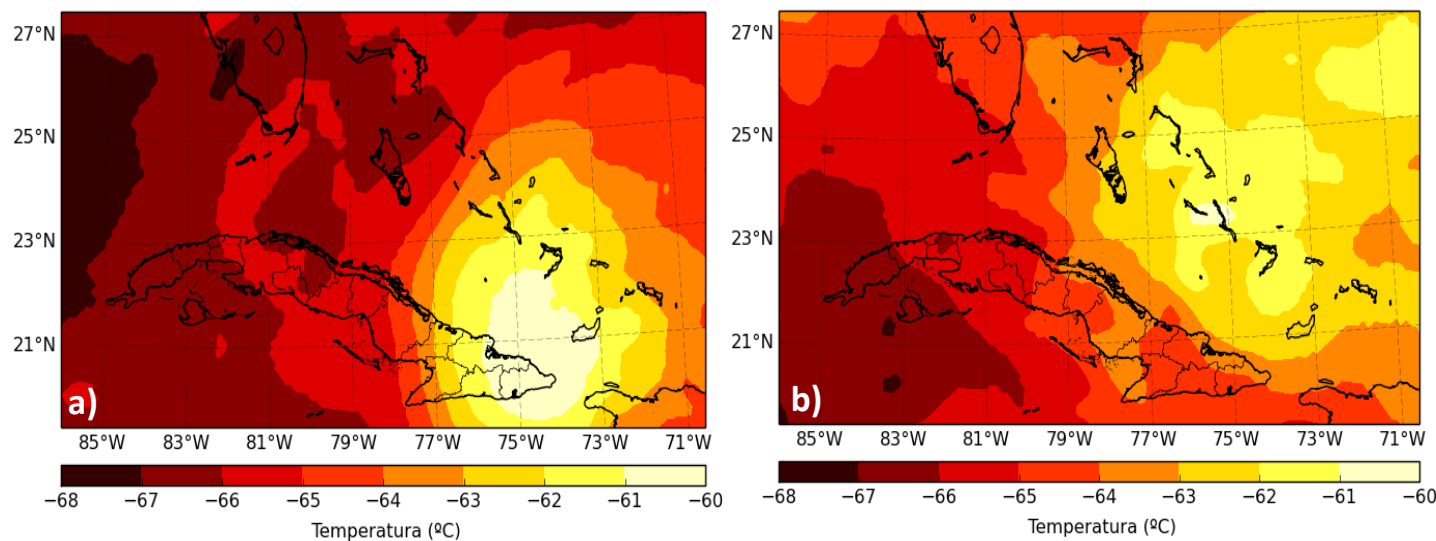


Figure 3.3: Temperature at the level at the 150 mb level corresponding to July 2, 2016 at 1400 UTC (a) and August 16, 2016 at 1300 UTC (b).

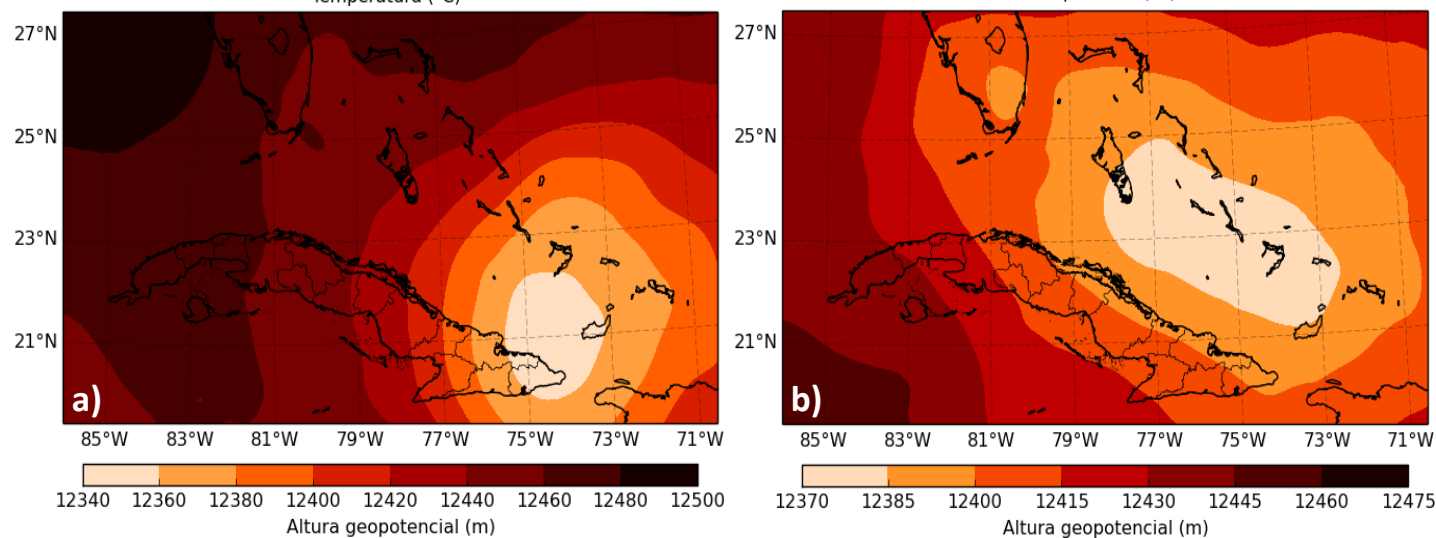


Figure 3.4: Geopotential height at the 200 mb level corresponding to July 2, 2016 at 1400 UTC (a) and August 16, 2016 at 1300 UTC (b).

Synoptic description

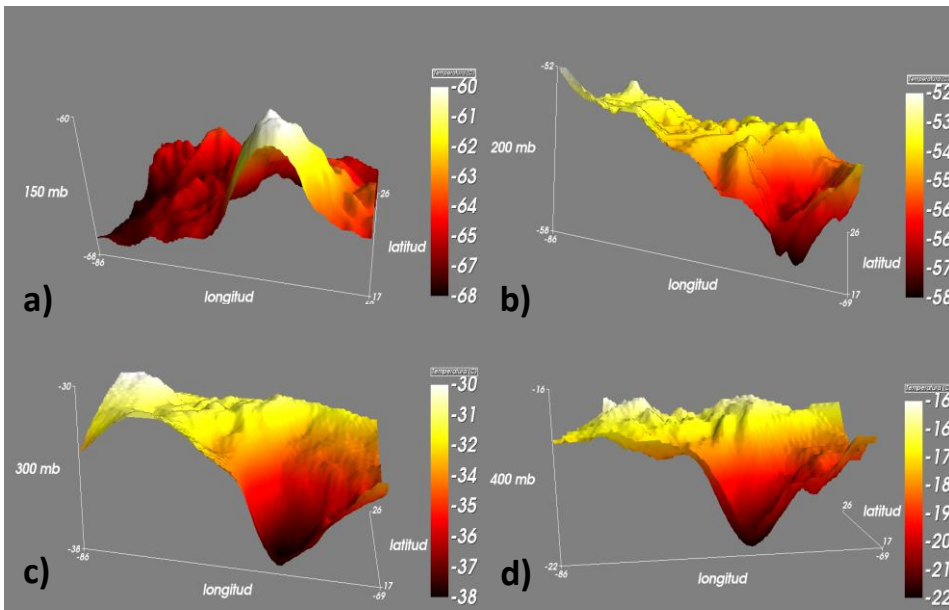


Figure 3.5: Temperature field for July 2, 2016 at 1400 UTC at the levels (a) 150 mb, (b) 200 mb, (c) 300 mb and (d) 400 mb.

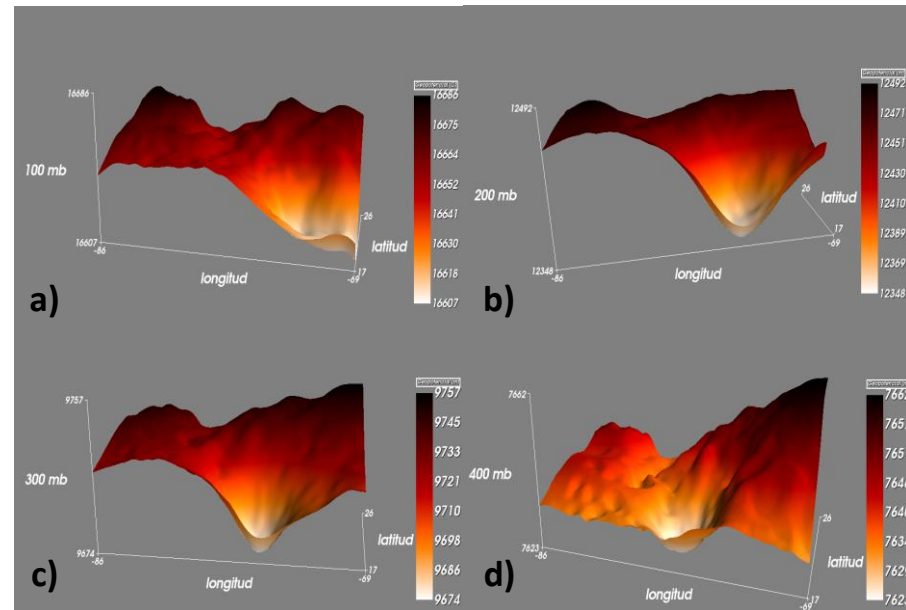


Figure 3.6: Geopotential height field for July 2, 2016 at 1400 UTC at levels (a) 100 mb, (b) 200 mb, (c) 300 mb and (d) 400 mb.

Synoptic description

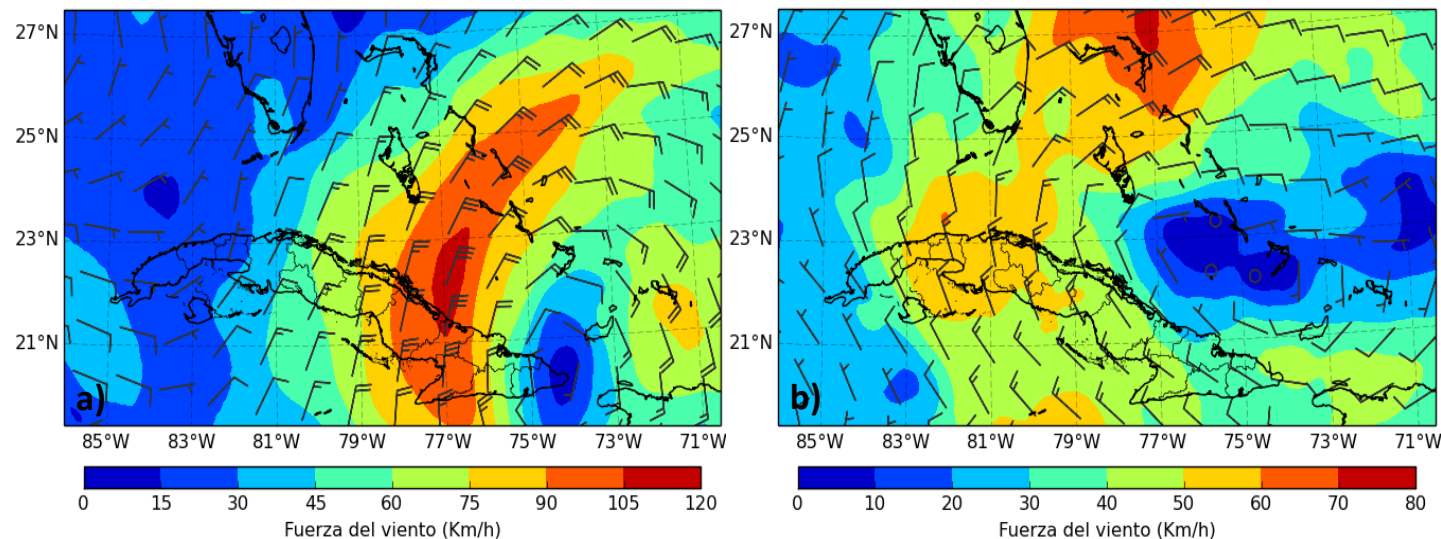


Figure 3.7: Wind speed and direction at the 200 mb level corresponding to July 2, 2016 at 1400 UTC (a) and August 16, 2016 at 1300 UTC (b).

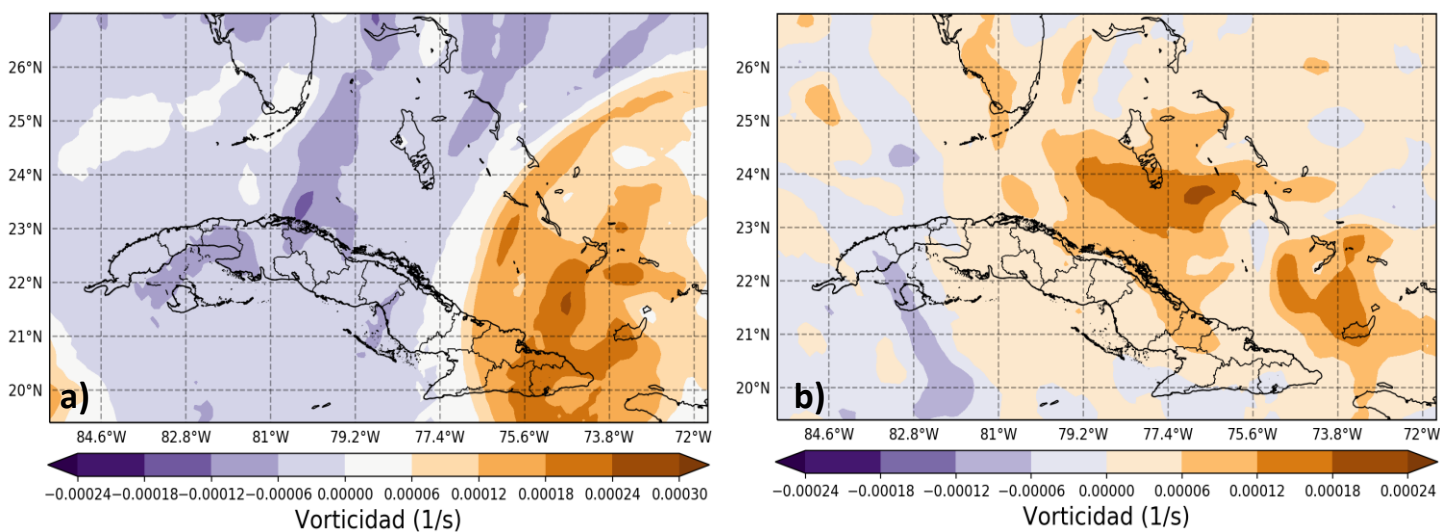


Figure 3.8: Vorticity at the 200 mb level corresponding to July 2, 2016 at 1400 UTC (a) and August 16, 2016 at 1300 UTC (b).

Synoptic description

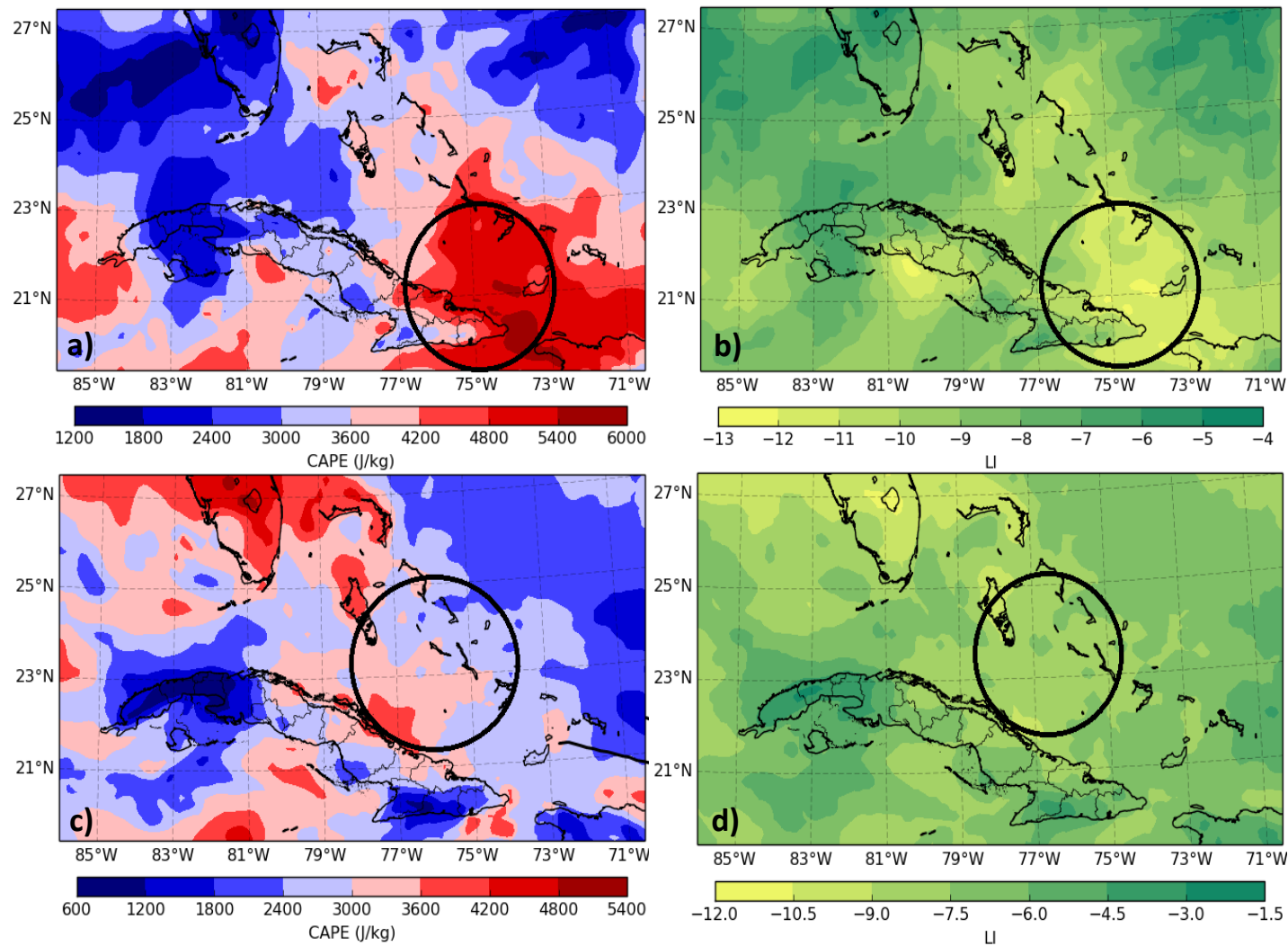


Figure 3.9: CAPE and LI values at the 200 mb level corresponding to July 2, 2016 at 2200 UTC ((a) and (b)) and August 16, 2016 at 1400 UTC ((c) and (d)).

Synoptic description

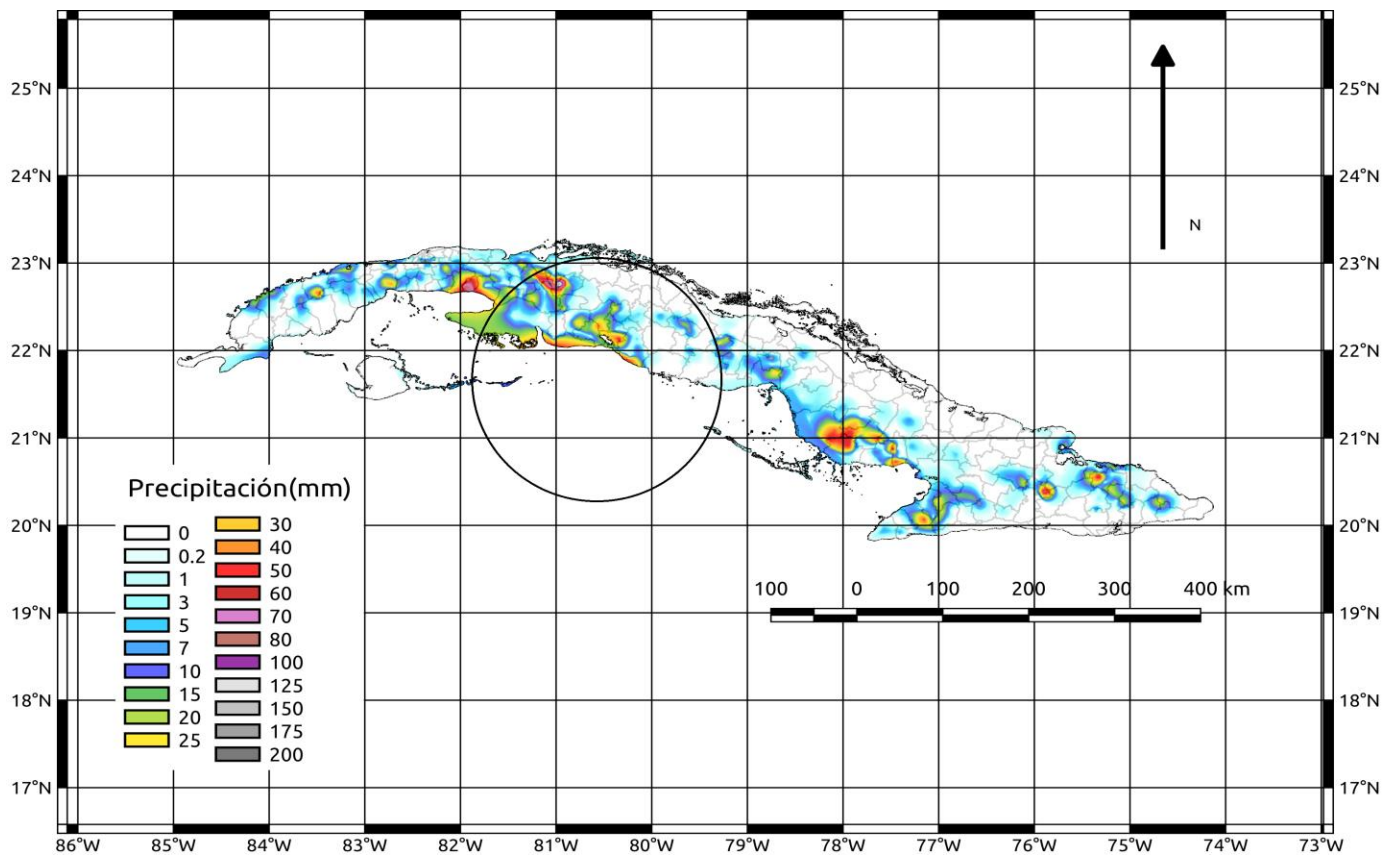


Figure 3.10: Accumulated precipitation for July 3, 2016.

Analysis of satellite images

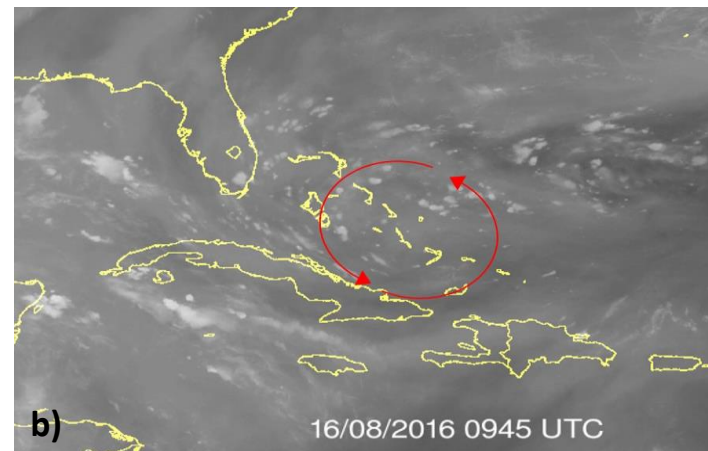
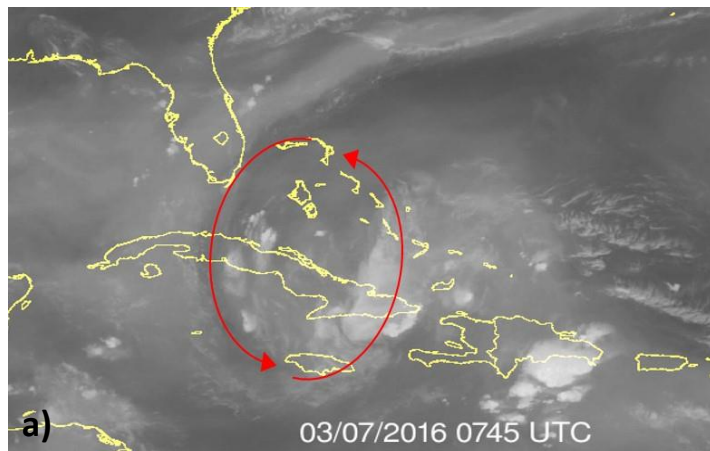


Figure 3.11: Satellite image on the WV channel, where the UCLs are observed for July 3, 2016 at 0745 UTC (a) and August 16, 2016 at 0945 UTC (b).

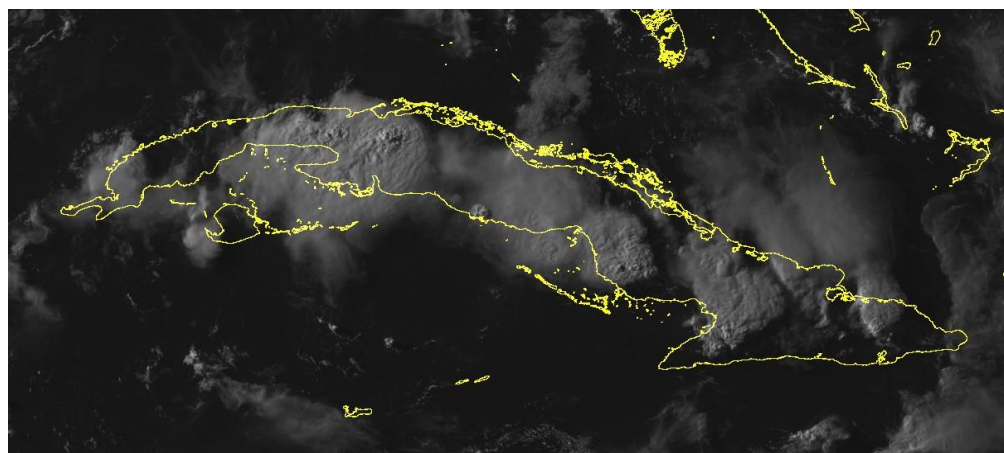


Figure 3.12: Satellite image (visible channel) corresponding to July 2, 2016 at 2215 UTC showing deep convection.

Analysis of radar observations

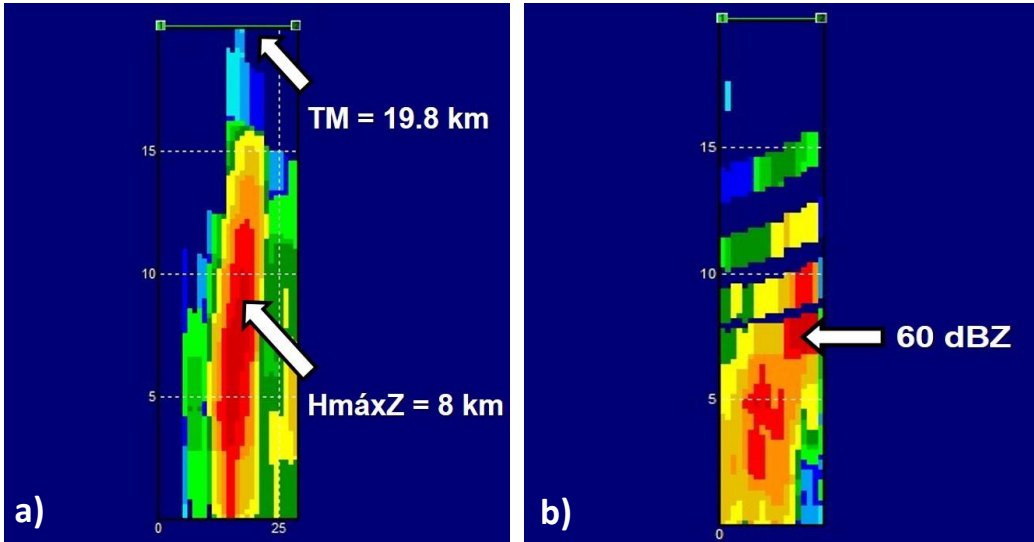


Figure 3.13: Vertical section of two convective cells corresponding to July 2, 2016 at 1850 UTC (a) and August 17, 2016 1620 UTC (b).

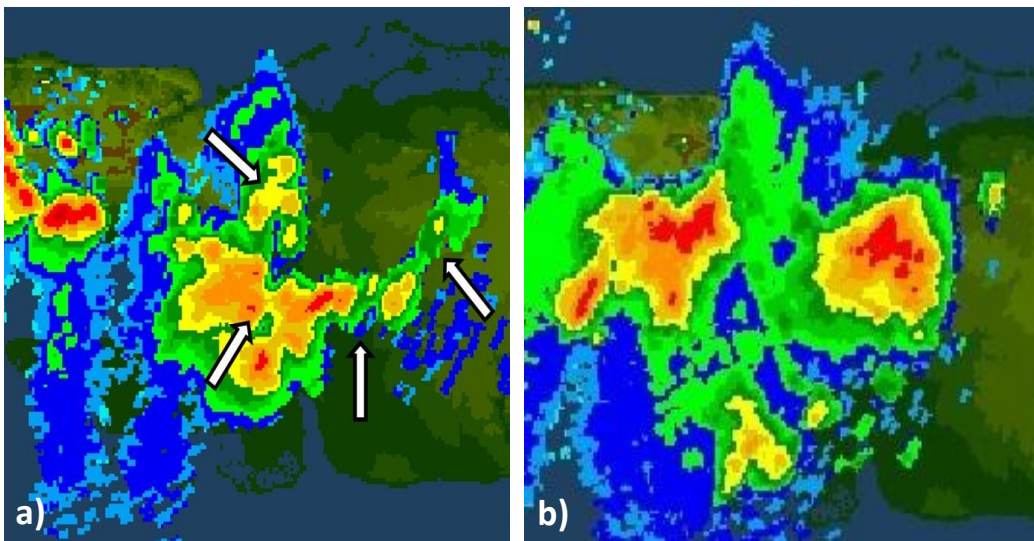


Figure 3.14: Radar observation corresponding to July 3, 2016 where the emergence of new convective cells is observed from the streak front of a dissipating storm. (a) 17:20 UTC and (b) 18:30 UTC.

Mesoscale analysis of variables and indices from the WRF model

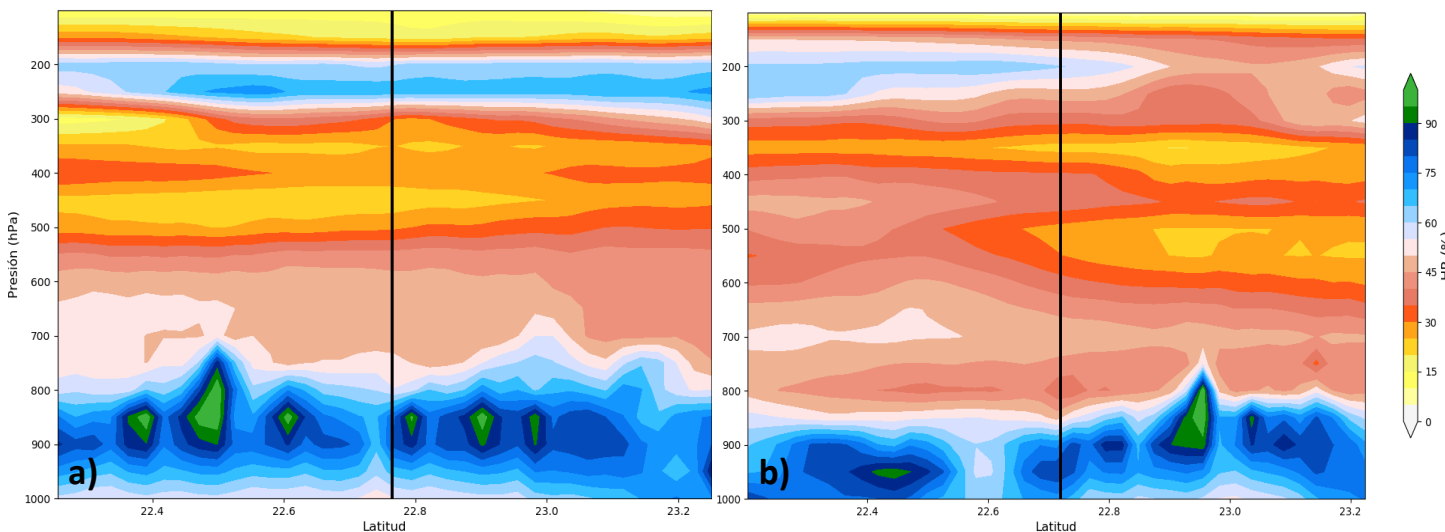


Figure 3.15: Southern vertical section of the relative humidity from the WRF corresponding to July 3, 2016 at 1800 UTC (a) and August 17 at 1700 UTC (b).

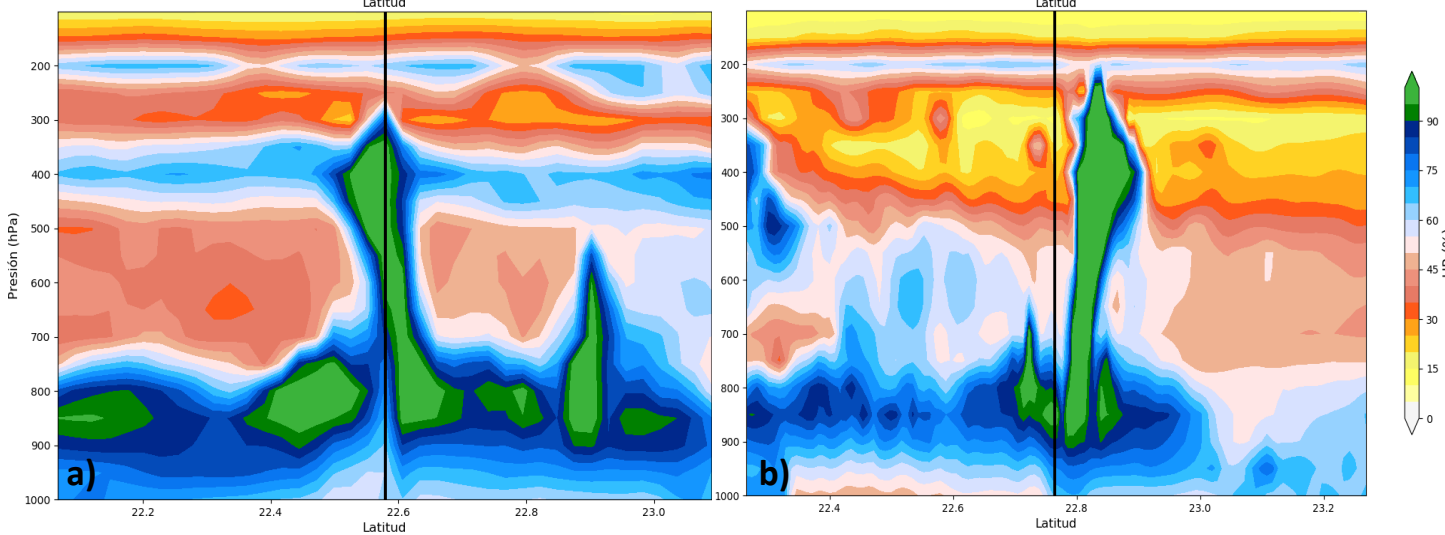


Figure 3.16: Southern vertical section of the relative humidity from the WRF corresponding to July 2, 2016 at 2300 UTC (a) and July 3, 2016 at 2100 UTC (b).

Mesoscale analysis of variables and indices from the WRF model

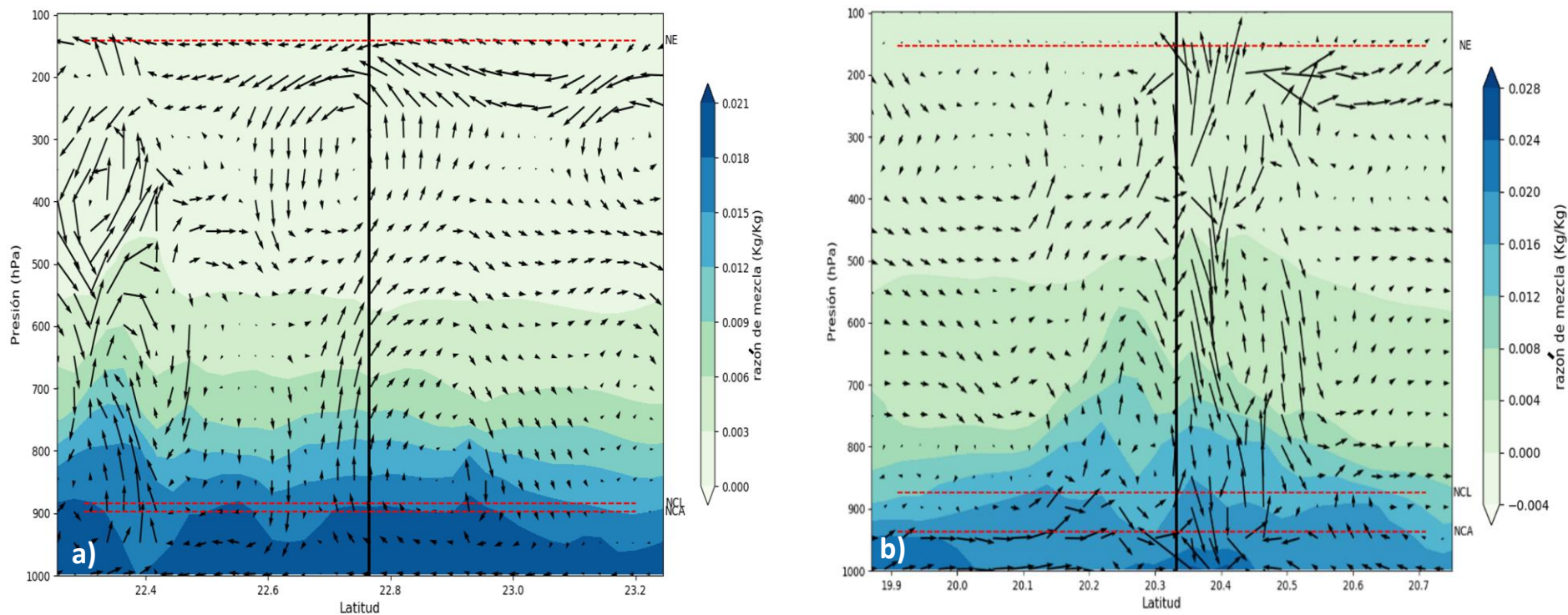


Figure 3.17: Southern vertical section of the mixing ratio (kg / kg) with the wind direction from the WRF corresponding to July 3, 2016 at 2200 UTC (a) and August 16, 2016 at 1900 UTC (b).

Mesoscale analysis of variables and indices from the WRF model

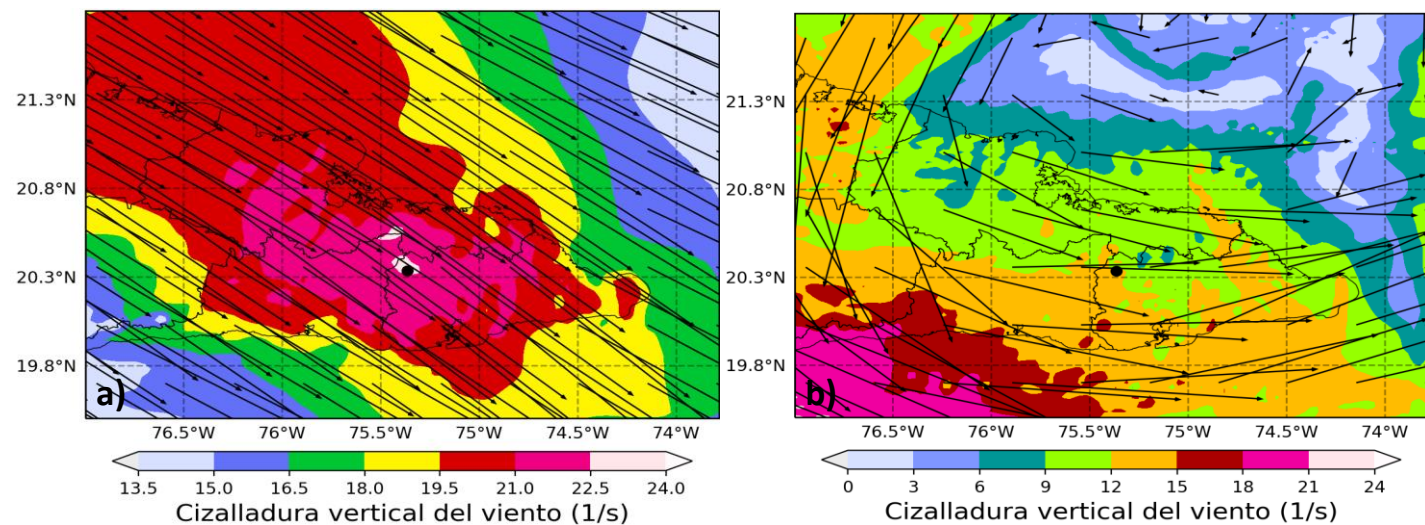


Figure 3.18: Vertical wind shear in the 850 - 200 mb layer from the WRF corresponding to August 16, 2016 at 0100 UTC (a) and 1600 UTC (b).

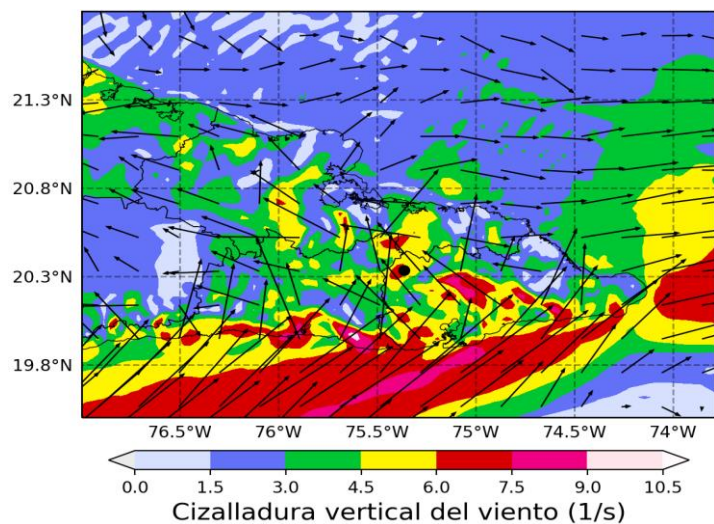


Figure 3.19: Vertical wind shear in the sfc layer - 500 mb from the WRF corresponding to August 16, 2016 at 1100 UTC.

Conclusions

1. The presence of the Upper Cold Lows generated an unstable and potentially favorable synoptic environment for the development of deep convection, with vertical temperature gradients greater than 6.7×10^{-3} ($^{\circ}\text{C} / \text{m}$) in the afternoon between the surface and the level of 500 mb. The CAPE showed extreme values higher than 6000 J / kg near the center of the system and the LI reached -13. Furthermore, the relative vorticity at the 200 mb level ranged between 2.5×10 (s^{-1}) and 3.94×10^{-3} (s^{-1}) in the right sector of the Upper Cold Lows, while the vertical velocity described upward movements to the south and east of the system with values between -1.97 Pa / s and -3.76 Pa / s.
2. The humid Upper Cold Low was characterized by being more intense than the dry one and, although the direct influence of both increased the temporal distribution of rainfall in Cuba, it was higher with the humid Upper Cold Lower. The highest accumulated were reported near the center of both systems. The highest number of reports of locally intense rain occurred in the western region of the lowlands, with three of the four cases analyzed, behavior similar to that of other dangerous phenomena such as Severe Local Storms.

Conclusions

3. According to the output of the WRF model, the cases of intense rain studied were generated in an environment of weak vertical wind shear in the middle and lower troposphere, being moderate to strong in the upper troposphere. High relative humidity values greater than 70% predominated in the surface layer - 800 mb and a dry layer between 700 and 300 mb with values less than 45%. The temperature at 500 mb ranged between -6 and -10 ° C and the 0 ° C isotherm was located slightly above 600 mb. Regarding CAPE, it was above 2300 J / kg in the four cases, with an LI that varied between -5 and -10.
4. The interaction of the pre-existing storm surge fronts or the sea breeze front with the HCRs was the main trigger for deep and organized convection. The storms that were generated were characterized by presenting maximum reflectivity values greater than 50 dBz in the four cases analyzed, the tops were greater than 12 km in height, exceeding 19 km in two of the cases and the maximum reflectivity height ranged between 3 and 5 km. In all cases, the locally intense rain was generated by the influence of several convective cells. The Batabanó case was affected by four cells, while Colón and La Sierpe by five and three respectively. Using the 1 km spatial resolution of the WRF model, they were able to determine upward velocities within the cloud that reached 24 m / s.